A comparison between two approaches for calculating power spectral densities of ground-borne vibration from railway trains

E. Ntotsios[1], M.F.M. Hussein[1], D.J. Thompson[1]
[1]Institute of Sound and Vibration Research, Faculty of Engineering and the Environment, University of Southampton, Highfield, Southampton SO17 1BJ, UK
email: e.ntotsios@soton.ac.uk, m.hussein@soton.ac.uk, djt@isvr.soton.ac.uk

ABSTRACT: Ground-borne vibration from railways is generated at the wheel-rail interface due to the passage of individual wheels along tracks and due to irregularities of wheels and tracks. In this paper, two approaches are used to calculate the vibration Power Spectral Density (PSD) in the free field from a train moving on a surface railway track at a constant velocity. They both use the PSD of the track unevenness along with Transfer Functions (TFs) of the track and its supporting ground that are calculated using a well-developed 2.5D semi-analytical model which accounts for a ballasted track on the surface of a homogeneous layered half-space. The first approach is based on modelling a train at fixed position on the track which is excited by 'moving roughness'; the roughness is pulled through between the wheels and track with the velocity of train, assuming that each wheel is excited by the same roughness apart from a time lag. In the second approach the motion of the train is included which means that the response at a given frequency is a combination of responses induced by different excitation frequencies due to the Doppler effect in the ground. For both approaches mathematical expressions are used to predict the average dynamic response directly. The paper compares the dynamic response calculated by each approach for a range of train/ground parameters and highlights the computational effort needed by each approach. It also shows the effect of approximations adopted in the first approach on the accuracy of predictions. The predictions calculated by the two approaches are verified using a coupled 2.5D finite element/boundary element model.

KEY WORDS: Ground-borne vibration; Surface railways; Free field wave propagation.

1 INTRODUCTION

Ground-borne vibration from railways is a problem that affects residents and sensitive equipment in buildings near railway lines. Ground-borne vibration from railways is generated at the wheel-rail interface due to the passage of individual wheels along tracks (quasi-static loading) and due to irregularities of wheels and tracks (dynamic loading). Vibration propagates to nearby buildings where it causes annoyance to people and malfunctioning of sensitive equipment. Inhabitants of buildings perceive vibration either directly, due to motion of floors and walls, or indirectly as re-radiated noise.

Modelling ground-borne vibration from railways is essential for understanding the physics of its generation and propagation. A good understanding of the problem is key to identifying ways to tackle unacceptable levels of vibration from existing as well as future railway lines. A large number of numerical models for predicting vibration from surface and underground railways have been presented in the literature. By coupling sub-models for the train, the track and the soil, the resulting prediction models range from simple multi-degree-of-freedom models to two-dimensional and more comprehensive three-dimensional models. The latter have received more attention due to their closer representation of the real problem and therefore their better potential accuracy compared with other models. In these models, the geometry of the track and the soil is often assumed to be invariant in the longitudinal direction of the track. This allows the use of efficient "two-and-a-half dimensional" (2.5D) solution procedures, based on a Fourier transform with respect to the coordinate along the track. Alternative methods based on the finite element method require appropriate procedures to account for the unbounded domain and to avoid spurious reflections at boundaries. A comprehensive overview of the state of the art on railway induced ground vibration models can be found in [1].

A distinction is generally made between the quasi-static and dynamic excitation. The quasi-static excitation is related to the static (invariant with time) component of the moving axle loads whereas the dynamic excitation is determined by dynamic train-track interaction due to several excitation mechanisms, such as the wheel and track unevenness and the spatial variation of the support stiffness. The quasi-static contribution to the response generally remains important, however, only in the immediate vicinity of the track. It has been shown (e.g. [2] [3]) that the relative importance of quasi-static and dynamic excitation depends on the train speed, the ratio of the static and dynamic axle loads, and the dynamic characteristics of the track and the soil.

The dynamic wheel-rail forces are generated from the irregular vertical profiles of the wheel and rail running surfaces. The rail irregularities might include dipped joints and corrugations as well as general undulation in the 'track top'. The wheel irregularities can be wheel flats, surface irregularities and wheel eccentricity. The variations in the vertical profiles of either surface (wheel and rail) introduce a relative displacement input to the system. The process is assumed to be linear, so that for a given wavelength λ a displacement input is generated at the passing frequency $f = v/\lambda$ where v denotes the train speed. In the present

work, the wheels of the trains are assumed to be perfectly smooth, so that all irregularities are contained in the rail surface. This assumption ignores the effect of wheel irregularities that are bound to exist on real trains and that is likely to weaken the degree of coherence between axle inputs, especially at shorter wavelengths. Nonetheless, the smooth-wheel assumption is a useful starting point for a more realistic input excitation in comparing the effectiveness of various ground-borne vibration prediction models.

Vibration from railways can be treated as a random process. When the vibration is calculated at a point that is moving with the speed of the train (moving frame) the vibration can be considered as stationary process. One of the common outputs normally considered from the models is the PSD of vibration at measurement points. The PSD helps in identifying the main frequency components contributing to the total vibration. It also helps in relating those frequencies to the excitation mechanisms and the dynamics of the track and transmitting ground.

There are two common approaches reported in the literature for calculating the PSD from a train moving at a constant velocity. They both use the PSD of the track unevenness along with Transfer Functions (TFs) of the track and the supporting ground. The first approach is based on modelling a train at fixed positions on the track which are excited by a "moving roughness"; the roughness is pulled through between the wheels and track with the velocity of train, assuming that each wheel is excited by the same roughness apart from a time lag. In the second approach, vibration is calculated at a fixed point for the moving train which means that the response at a given frequency is a combination of responses induced by different excitation frequencies due to the Doppler effect in the ground. Mathematical expressions are used to give directly the average response during the pass-by.

In this paper, these two approaches have been used to calculate the vibration PSD in the free field from a train moving on a surface railway track. The TFs of the track and its supporting ground are calculated using a 2.5D semi-analytical model developed by Sheng et al. in [4]. The model accounts for a ballasted track on the surface of a homogeneous layered half-space. The paper compares results calculated by each approach for a range of practical train parameters and velocities and highlights the computational effort needed by each approach. This is used to show the effect of approximations made on the accuracy of the two approaches. The predictions calculated by the two approaches are verified using a coupled 2.5D finite element/boundary element model developed in [6].

2 THE NUMERICAL PREDICTION MODEL

In this section, the receptances of a vehicle and a track-ground system are presented. For ground-borne vibrations where the frequency range of interest is usually between 0 and 100 Hz, the vehicle is modelled as a multiple-body system and a Hertzian contact spring is introduced between each wheelset and the rail. The car body of the vehicle has six degrees of freedom (DOFs), accounting for three displacements of the mass centre and three rotations around three orthogonal axes. As only the vertical dynamics of the vehicle are considered (i.e. in the $x-z$ plane where z is vertically downwards and x is along the rail; Figure 1), then each body has only two degrees of freedom, i.e., the vertical displacement of its mass centre and its pitch motion (see Figure 2a). In practice, the suspensions in the vehicle may have non-linear behaviour. However, to enable analysis in the frequency domain, here, each non-linear suspension is linearized. As a result, the differential equation of motion for the vehicle is linear with constant coefficients and is specified by a mass matrix $\mathbf{M}_V$ and a stiffness matrix $\mathbf{K}_V$. Damping is introduced and included in the stiffness matrix, thus the elements of the stiffness matrix are complex and frequency dependent. The mass and stiffness matrices of several typical vehicles are presented in [2].

The vertical forces between the wheelsets and the rails are denoted, from the first wheelset of the first vehicle to the last wheelset of the last vehicle, by $\boldsymbol{P}(t)=\{P_1(t)\ldots P_M(t)\}^{\mathrm{T}}$, where M is the number of the forces. As only vertical dynamics are included, the forces are not separated into their components on the two rails. The longitudinal co-ordinates of these forces are denoted by $\alpha_1,\alpha_1,\ldots,\alpha_M$. For each wheel–rail force, there are two components: one is a moving 'quasi-static' load, i.e., the moving axle load, and the other is a moving dynamic load. The responses to the axle loads are independent of vehicle dynamics. Therefore only the dynamic wheel-rail forces are considered here; in the following, $\boldsymbol{P}$ refers to these dynamic forces. The vertical displacement of the rail is denoted by $w_R(x,t)$. For positions on the ground surface, the vertical (z-direction) displacement is denoted by $w_G(x,y,t)$.

2.1 The train-track interaction problem

The differential equation of motion of a single vehicle is given by

$$\mathbf{M}_V\ddot{\boldsymbol{w}}_V(t)+\mathbf{K}_V\boldsymbol{w}_V(t)=-\mathbf{B}\boldsymbol{P}_V(t) \tag{1}$$

where $\boldsymbol{w}_V(t)$ denote the displacement vector, $\mathbf{B}$ is a matrix of unit and zero elements [2] and $\boldsymbol{P}_V(t)$ is the wheel-rail force vector for this vehicle, being a subvector of $\boldsymbol{P}(t)$. The minus sign before $\boldsymbol{P}_V(t)$ indicates that the positive wheel-rail forces correspond to compression of the contact spring.

By setting $\boldsymbol{P}_V(t)=\tilde{\boldsymbol{P}}_V(\omega)e^{i\omega t}$ and $\boldsymbol{w}_V(t)=\tilde{\boldsymbol{w}}_V(\omega)e^{i\omega t}$ where ω denotes the angular frequency Eq. (1) yields

$$\tilde{\boldsymbol{w}}_V(\omega)=-\left(\mathbf{K}_V-\omega^2\mathbf{M}_V\right)^{-1}\mathbf{B}\tilde{\boldsymbol{P}}_V(\omega)=-\boldsymbol{\Sigma}_V\tilde{\boldsymbol{P}}_V(\omega) \tag{2}$$

where $\boldsymbol{\Sigma}_V=\left(\mathbf{K}_V-\omega^2\mathbf{M}_V\right)^{-1}\mathbf{B}$ is an $M\times M$ matrix of receptances (displacements due to a unit force) of the vehicle DOFs at the wheelsets.

The displacement vector of the wheelsets produced by the wheel-rail forces in a single vehicle is given by

$$\tilde{\boldsymbol{w}}_W(\omega)=-\boldsymbol{\Sigma}_W\tilde{\boldsymbol{P}}_V(\omega) \tag{3}$$

where $\boldsymbol{\Sigma}_W$ is the receptance matrix at the wheelsets for a single vehicle given by

$$\boldsymbol{\Sigma}_W = \begin{bmatrix} \sigma_{11}^W & \cdots & \sigma_{1N}^W \\ \vdots & \cdots & \vdots \\ \sigma_{N1}^W & \cdots & \sigma_{NN}^W \end{bmatrix} = \mathbf{B}^{\mathrm{T}} \left(\mathbf{K}_V - \omega^2 \mathbf{M}_V \right)^{-1} \mathbf{B} . \qquad (4)$$

The receptance between the j th and the k th wheelsets within a vehicle is denoted in Eq. (4) by σ_{jk}^W with $j,k = 1,2,\ldots,N$; N being the number of wheelsets of the vehicle. These receptances denote the displacement amplitude of the j th wheelset due to a unit vertical harmonic load of frequency ω exerted at the k th wheelset.

Supposing that the whole train consists of N_1 identical vehicles the total number of the wheel-rail forces is $M = N_1 N$. Assuming that the vehicles are coupled only by the rails, then the receptance matrix at the wheelsets for the train, denoted by $\boldsymbol{\Sigma}_T$, is given by

$$\boldsymbol{\Sigma}_T = \mathrm{diag}\left(\boldsymbol{\Sigma}_W \right) = \begin{bmatrix} \boldsymbol{\Sigma}_W & \cdots & 0 \\ \vdots & \ddots & \vdots \\ 0 & \cdots & \boldsymbol{\Sigma}_W \end{bmatrix} . \qquad (5)$$

By considering an infinite rail, the receptance σ_{jk}^R at the j th wheel-rail contact point due to a unit load at the k th wheel-rail contact point is determined by

$$\sigma_{jk}^R = w_R(l_{jk}) \qquad (6)$$

where $l_{jk} = \alpha_j - \alpha_k$ is the longitudinal distance between the two contact points, and when the j th contact point is ahead of the k th contact point $l_{jk} > 0$. The displacement of the rail $w_R(x)$ in (6) is given in the next Section by coupling the track to the ground model.

By denoting the receptance matrix of the track–ground system at the wheel–rail contact points as

$$\boldsymbol{\Sigma}_R = \begin{bmatrix} \sigma_{11}^R & \cdots & \sigma_{1M}^R \\ \vdots & \cdots & \vdots \\ \sigma_{M1}^R & \cdots & \sigma_{MM}^R \end{bmatrix} . \qquad (7)$$

The displacement vector at the wheel-rail contact points on the rails at frequency ω is given by

$$\tilde{\boldsymbol{w}}_R(\omega) = \boldsymbol{\Sigma}_R \tilde{\boldsymbol{P}}(\omega) . \qquad (8)$$

The coupling of a wheelset with the rails is illustrated in Figure 1, where $\tilde{w}_{Wl}(\omega)e^{i\omega t}$ denotes the displacement of the l th wheelset and $\tilde{w}_l(\omega)e^{i\omega t}$ denotes the complex amplitude of the vertical profile of the rail (rail irregularity) at the contact point. The vertical profile of the rail may be decomposed into a spectrum of discrete harmonic components. A single harmonic component is denoted by $w(x) = Ae^{i(2\pi/\lambda)x}$ where λ denotes the wavelength and A the amplitude which may be complex. The relation between the angular frequency of the dynamic loading and the wavelength of the rail irregularity is $\omega = 2\pi v/\lambda$.

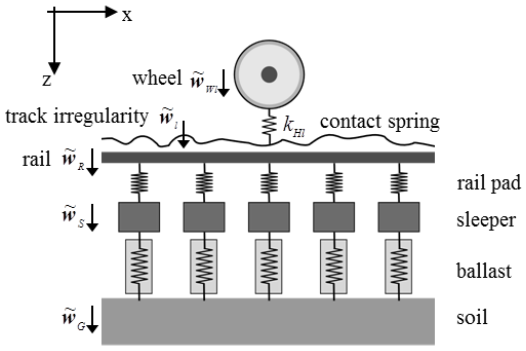

Figure 1. Coupling of the l th wheelset with the track (rail, pad, sleeper, ballast) and the ground.

A Hertzian contact spring is inserted between the wheelset and the rails. The stiffness of the Hertzian contact spring is denoted by k_{Hl}. It is assumed that the wheelset is always in contact with the rails, thus

$$\tilde{w}_{Wl}(\omega) = \tilde{w}_{Rl}(\omega) + \tilde{w}_l(\omega) + \tilde{P}_l(\omega)/k_{Hl} . \qquad (9)$$

From Eq. (3) and Eq. (8)

$$\tilde{w}_{Wl}(\omega) = -\sum_{k=1}^{M} \sigma_{lk}^T \tilde{P}_l(\omega) \qquad (10)$$

$$\tilde{w}_{Rl}(\omega) = \sum_{k=1}^{M} \sigma_{lk}^R \tilde{P}_l(\omega) \qquad (11)$$

by denoting σ_{lk}^T the elements of matrix $\boldsymbol{\Sigma}_T$ in (5) for $k,l = 1,2,\ldots,M$. Inserting these two equations into Eq. (9) yields

$$\sum_{k=1}^{M} \left(\sigma_{lk}^T + \sigma_{lk}^R \right) \tilde{P}_k(\omega) + \frac{1}{k_{Hl}} \tilde{P}_l(\omega) = -\tilde{w}_l(\omega) \qquad (12)$$

with $(l = 1,2,\ldots,M)$.

Eq. (12) is a set of linear algebraic equations with unknowns the dynamic wheel-rail forces $\tilde{\boldsymbol{P}}(\omega)$. The solution of Eq. (12) will be used as an input for the coupled track-soil model to give the response of the rail and in the free field.

2.2 The track-soil interaction problem

The railway track is aligned in the x direction and has an invariant contact width $2b$ with the ground (see Figure 2b). Different railway structures may be represented by different models having the same form. In this work, a track structure comprising rail, rail pad, sleeper and ballast is presented (see Figure 1). The two rails are represented as a single Euler-Bernoulli beam and the rail pads are modelled as a distributed vertical stiffness. The sleepers are modelled as a continuous mass per unit length of the track and the ballast is modelled as continuous distributed vertical spring stiffness with consistent mass. An embankment, if present, can be modeled in the same way as the ballast.

The track is assumed to be located at the surface of a horizontally layered half-space, with a geometry that is invariant in the longitudinal direction x. For the aims of this paper an efficient 2.5D semi-analytical model developed by Sheng et al. in [4] will be used for the prediction of the ground response excited by harmonic loads acting directly on the ground, or, as shown in Figure 2b, for loads acting via a coupled track structure. The model which is based on the flexibility matrix approach uses the Fourier transform in the wavenumber domain β, γ with respect to the coordinates x, y along and normal to the track. The coupling of the ground with the railway track is carried out by taking into account the continuity of the displacements and the equilibrium of the stresses in the plane of contact between them, rendering it possible to calculate the Fourier transformed response of the ground surface and the track elements.

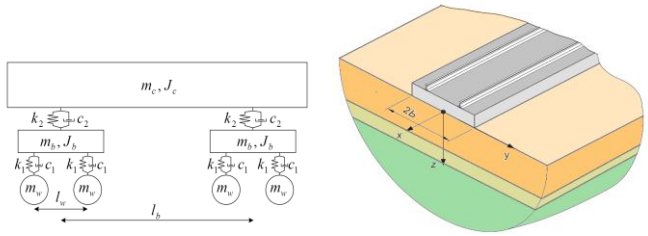

(a) (b)

Figure 2. (a) 10 DOF multi-body model of vehicle and (b) the geometry of the coupled track-soil system and

2.2.1 The response due to stationary harmonic loads

Following the analysis in [4] for a coupled track-ground system and introducing the TF $H_G^0(x-\alpha_l, y, \omega)$ for the response at a point x, y at the ground surface due to stationary unit harmonic load of angular frequency ω acting at $x=\alpha_l$, the displacements of the ground surface (in the vertical direction) due to a series of M harmonic loads of amplitude P_l $(l=1,2,\ldots,M)$ positioned at $\alpha_1, \alpha_1, \ldots, \alpha_M$ is denoted as

$$w_G(x,y,t)=\sum_{l=1}^{M} H_G^0(x-\alpha_l, y, \omega)P_l(\omega)e^{i\omega t} \qquad (13)$$

and the displacements of the rail as

$$w_R(x,t)=\sum_{l=1}^{M} H_R^0(x-\alpha_l, \omega)P_l(\omega)e^{i\omega t}\,. \qquad (14)$$

These TFs as functions of Cartesian co-ordinates are derived through a two (one for the rail) dimensional inverse FFT, or a Fourier transform implemented through a standard quadrature respectively, i.e.

$$H_G^0(x-\alpha_l, y, \omega)=\frac{1}{4\pi^2}\int_{-\infty}^{\infty}\int_{-\infty}^{\infty}\tilde{H}_G^0(\beta,\gamma,\omega)e^{i(\beta x+\gamma y)}\mathrm{d}\beta\mathrm{d}\gamma\,. \qquad (15)$$

The semi-analytical expressions for the TFs i.e. $\tilde{H}_G^0(\beta,\gamma,\omega)$ in the wavenumber domain β, γ can be found in [4].

2.2.2 The response due to moving loads

In [5] this model has been extended to encompass the effect of loads moving on the track. The model deals with both moving loads that are constant and also those that have a non-zero frequency. Assuming that all loads move with the same speed the solution in this case is achieved in a frame of reference moving with each load.

The semi-analytical expressions for the TFs in the wavenumber domain β, γ available in [5] which are derived for a moving frame of reference can give the TFs in the spatial domain by inverse Fourier Transform:

$$H_G(x-\alpha_l-vt, y, \hat{\omega})=\frac{1}{4\pi^2}\int_{-\infty}^{\infty}\int_{-\infty}^{\infty}\tilde{H}_G^0(\beta,\gamma,\omega-\beta v)e^{i(\beta x+\gamma y)}\mathrm{d}\beta\mathrm{d}\gamma \qquad (16)$$

for the ground surface and

$$H_R(x-\alpha_l-ct, \hat{\omega})=\frac{1}{2\pi}\int_{-\infty}^{\infty}\tilde{H}_R(\beta,\omega-\beta v)e^{i\beta x}\mathrm{d}\beta \qquad (17)$$

for the rail. These TFs are calculated for receiving frequencies $\hat{\omega}=\omega-\beta v$ and denote the displacement for a fixed point x, y at the ground surface due to a unit moving load of angular frequency ω acting at $x=\alpha_l$, where the coupling between the position $x=\alpha_l-vt$ of the k th axle and the load gives rise to Doppler effect.

The displacement of the ground due to a sequence of M loads of amplitude P_l $(l=1,2,\ldots,M)$ is given by

$$w_G(x,y,t)=\sum_{l=1}^{M} H_G(x-\alpha_l-vt, y, \hat{\omega})P_l(\omega)e^{i\omega t}\,. \qquad (18)$$

Similarly the displacement of the rail is

$$w_R(x,y,t)=\sum_{l=1}^{M} H_R(x-\alpha_l-vt, \hat{\omega})P_l(\omega)e^{i\omega t}\,. \qquad (19)$$

It should be emphasized, that although the load is applied with a single non-zero frequency or at zero frequency, the ground vibration is a transient with a broad frequency content. In order to calculate the spectrum of the response of the ground or the rail to the moving load of single angular frequency ω, Eqs. (18) and (19) are Fourier transformed with respect to time t. It should be noted that the amplitude of resulted response spectrum are independent of the value of x. This reflects the fact that the spectrum represents the movement through the observation point of the steady state wave field associated with the load moving along the x-axis from $x=-\infty$ to $x=+\infty$.

Note that for the case of constant moving loads the relations in (18) and (19) can give the quasi-static response due to the moving axle loads of a train by setting the excitation frequency $\omega=0$.

3 RESPONSE PSD IN THE FREE FIELD

Since vibration from railways when calculated at a point that is moving with the speed of the train can be treated as a stationary random process, one of the outputs normally

considered from the models is the PSD of vibration at measurement (observation) points. In this Section two approaches are presented for calculating the PSD in the free field from a train moving at a constant velocity. They both use the PSD of the track unevenness along with TFs of the track and the supporting ground introduced in Section 2.

3.1 The moving-roughness approach

This approach calculates the PSD of the response at a fixed (measuring) point on the ground surface by modelling a set of wheels at fixed positions on the track. For this case the roughness is assumed to be pulled through between the wheels and track with the velocity of train, assuming that each wheel is excited by the same roughness apart from a time lag. Since the loads in this approach are assumed as stationary and harmonic, the relations introduced in Section 2.2.1 will be used.

The vertical profile of the rail may be decomposed into a spectrum of discrete harmonic components. By assuming that the rail irregularity is moving with a speed v, at time t a unit amplitude irregularity of wavelength λ, denoted as $w(x) = e^{i(2\pi/\lambda)x}$, arrives at the l th wheelset at $x = \alpha_l$. Thus the displacement input at the l th wheel-rail contact point is

$$w_l(t) = \tilde{w}_l(\omega) e^{i\omega t} = e^{i(2\pi/\lambda)(\alpha_l + ct)} = e^{i(2\pi/\lambda)\alpha_l} e^{i(2\pi v/\lambda)t} \qquad (20)$$

where

$$\tilde{w}_l(\omega) = e^{i(2\pi/\lambda)\alpha_l} \qquad (21)$$

with $\omega = 2\pi v/\lambda$.

Thus, the dynamic vector of wheel-rail forces $\tilde{\boldsymbol{P}}(\omega)$ in (12) due to the unit amplitude rail irregularity $\tilde{w}_l(\omega)$ at all contact points can be calculated. The receptances σ_{jk}^R are given by Eq. (6) by considering a single unit amplitude load $P_l(\omega) = 1$ in Eq. (14).

A complete vertical rail profile made of a large number of discrete wavenumber components β_k is described by the Fourier series

$$w(x) = \frac{1}{2\pi} \sum_{k=-\infty}^{\infty} \tilde{w}(\beta_k) e^{i\beta_k x} \Delta\beta . \qquad (22)$$

where $\beta_k = k\Delta\beta$ and $\Delta\beta$ denotes the spacing of the discrete wavenumbers.

In this framework, the double-sided PSD of the displacement at a fixed observation point in the free field can be calculated by

$$S_G(x, y, \omega_k) = 2\left|H_G^0(x, y, \omega_k)\right|^2 S_{in}(\omega_k) . \qquad (23)$$

where $H_G^0(x, y, \omega_k)$ is the TF, which gives the displacement at the observation point due to a unit harmonic roughness of wavelength $\lambda_k = 2\pi v/\omega_k$ pulled through between all the wheelsets and the rail and $S_{in}(\omega_k)$ is the PSD of the vertical profile of the rail calculated at an angular frequency $\omega_k = v\beta_k$. The TF $H_G(x, y, \omega_k)$ is given by

$$H_G(x, y, \omega) = \sum_{l=1}^{M} H_G^0(x - \alpha_l, y) P_l(\omega_k) \qquad (24)$$

for the values of dynamic forces $P_l(\omega)$ calculated in (12). The factor of 2 in Eq. (27) arises from the fact that power spectrum of the rail profile is a single-sided function. More specifically the spectra discussed above are even (symmetric) functions of angular frequency, defined for frequencies from $-\infty$ to $+\infty$. However, in practice the power spectra are usually single-sided functions defined for positive frequencies only. If such single-sided spectra are used, they must still give the averaged value when integrated over all frequencies for which they are defined.

The velocity power spectrum, $S_{\dot{G}}(x, y, \omega_k)$, is given by

$$S_{\dot{G}}(x, y, \omega_k) = \omega_k^{\,2} S_G(x, y, \omega_k) \qquad (25)$$

In order to simulate the response at a point on the ground due to passing train, the averaged response for a line of points on the ground that has the same length with the train needs to be calculated. The average response is then given by

$$\bar{S}_G(y, \omega_k) = \frac{1}{L} \int_{\alpha_1}^{\alpha_M} S_G(x, y, \omega_k) \mathrm{d}x . \qquad (26)$$

where L is the length of the train.

When divided by the time taken for the whole train to pass a fixed point, Eq. (24) gives an estimate of the PSD of vibration at point x, y on the ground surface.

It should be noted that the formulation for the PSD in Eq. (23) already takes into account the correlation between the axles by introducing a time delay for the irregularity in (20). An alternative method for calculating the PSD has been introduced by Forrest and Hunt in [7] and implemented in the prediction model for an underground infinite railway. In this approach the power spectrum of the displacement at a fixed observation point in the free field can be calculated by

$$S_G(x, y, \omega_k) = 2\sum_{p=1}^{M}\sum_{q=1}^{M} H_G^{p\,*}(x, y, \omega_k) H_G^q(x, y, \omega_k) S_{in}(\omega_k) e^{i\omega_k(\alpha_q - \alpha_p)/v} \qquad (27)$$

where H^* denotes the conjugate of H. For this approach, each TF $H_G^j(x, y, \omega_k)$ in (27) is being calculated by Eq. (24) where the dynamic forces $P_l(\omega)$ are given in (12) by setting $\tilde{w}_l(\omega) = 1$ when $l = j$ and $\tilde{w}_l(\omega) = 0$ otherwise. This way the correlation between the axles is added at the right hand side of Eq. (27) by multiplying with the term $e^{i\omega_k(\alpha_q - \alpha_p)/v}$. Although this formulation will produce exactly the same PSD of response as Eq. (23), it allows the importance of axle correlation to be investigated if it is written as

$$S_G(x, y, \omega_k) = 2\sum_{p=1}^{M}\left|H_G^p(x, y, \omega_k)\right|^2 S_{in}(\omega_k) \qquad (28)$$

where by excluding the time delay for the irregularity the correlation between the axles is eliminated.

3.2 The full model for predicting the pass-by response

This section presents the formulation for the PSD of the ground surface response at a point that is stationary as the train moves past it. In this approach the motion of the train is included which means that the response at a given frequency is a combination of responses induced by different excitation frequencies due to the Doppler effect in the ground.

Following the analysis in [2] the vertical displacement spectrum of a point x, y on the ground surface due to a unit amplitude rail irregularity of wavelength λ, $w(x) = e^{i(2\pi/\lambda)x} = e^{i\beta x}$, is denoted by $S_0(x, y, f; \omega)$; where f is the frequency at which the spectrum is evaluated and ω is the excitation angular frequency determined by $\omega = 2\pi v/\lambda$.

At the time t, the l th wheelset arrives $x = \alpha_l + vt$, thus the displacement input at the l th wheel-rail contact point is given by the same expression as in Eqs. (20) and (21). Thus, the dynamic wheel-rail vector of forces $\tilde{\boldsymbol{P}}(\omega)$ in (12) due to the unit amplitude rail irregularity at all contact points $\tilde{w}_l(\omega)$ can be calculated. The receptances σ_{jk}^R in Eq. (6) are derived by considering a single unit amplitude load $P_l(\omega) = 1$ in Eq. (18). $S_0(x, y, f; \omega)$ may be obtained by Fourier transforming Eq. (18) with respect to time t.

Considering the rail profile of Eq. (22) ignoring the quasi-static effect, the power spectra of the ground surface response is given in [2] as

$$S_G(x, y, f) = \frac{1}{2\pi} \sum_{p=1}^{M} \left[\left| S_0(x, y, f; \omega_k) \right|^2 + \left| S_0(x, y, f; -\omega_k) \right|^2 \right] S_{in}(\beta_k) \Delta\beta_k \quad (29)$$

The velocity power spectrum, $S_{\dot{G}}(x, y, f)$, is given by

$$S_{\dot{G}}(x, y, f) = (2\pi f)^2 S_G(x, y, f) \quad (30)$$

When divided by the time taken for the whole train to pass a fixed point, equations (29) and (30) give an estimate of the PSD of vibration displacement and velocity respectively at point x, y on the ground surface.

4 NUMERICAL EXAMPLE

This section compares results calculated by each approach for a range of practical train parameters and velocities and highlights the computational effort needed by each approach. For this, two different types of soil are considered. The first soil has properties similar to a measurement site based on Horstwalde in Germany, which is a sandy soil that can be represented as a homogeneous half-space of moderately soft soil. The second is a layered half-space with a soft ground corresponding to a measurement site at Greby in Sweden [8]. The material properties chosen for the reference soil types are listed in Table 1.

For both soil cases the same track was used. More specifically, the track has bending stiffness per rail $EI = 6.4\,\text{MN}\cdot\text{m}^2$, mass per unit length per rail $m_R = 60\,\text{kg/m}$, damping loss factor of the rail $\eta_R = 0.01$, railpad vertical stiffness per unit length $k_p = 1000\,\text{MN/m}^2$, railpad damping loss factor $\eta_R = 0.1$, sleeper mass per unit length $m_S = 542\,\text{kg/m}$, ballast mass per unit length $m_B = 1740\,\text{kg/m}$, ballast stiffness per unit length $k_S = 4640\,\text{MN/m}^2$, ballast damping loss factor $\eta_R = 0.04$ and the width $2b$ of the contact interface between the track and the ground is $3.2\,\text{m}$. The rail unevenness profile for all simulations was chosen according to FRA class 3 [9]. This is plotted in Figure 3 in one-third octave bands (1/3 OB). It should be noted for a speed of 150 km/h and frequencies 1 to 100 Hz the corresponding wavelengths are $42\,\text{m}$ to $0.42\,\text{m}$.

Table 1. Soil properties for Horstwalde and Greby soils.

Site	Layer	Shear wave velocity [m/s]	Dilatation wave velocity [m/s]	Damping loss factor	Density [kg/m^3]	Thickness [m]
Horst-walde	Half space	250	1470	0.05	1945	-
Greby	1	103.36	193.37	0.2	1800	2
	2	122.30	228.80	0.2	1800	2
	Half space	310.09	580.12	0.2	2000	-

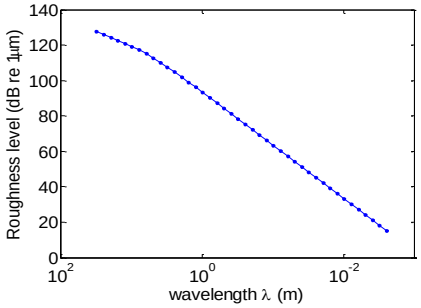

Figure 3. Assumed unevenness spectrum in 1/3 OB.

The train parameters used for both simulations are chosen to correspond to those used in [8]. These are based on a modified Bombardier Regina EMU ('Gröna Tåget'). Unlike [8] a four-car train is used with a total length of 106.4 m. Each vehicle (see Figure 2a) has car body mass $m_c = 40000\,\text{kg}$, car body pitching moment of inertia $J_c = 2\cdot10^6\,\text{kg}\cdot\text{m}^2$, bogie mass $m_b = 5000\,\text{kg}$, bogie pitching moment of inertia $J_b = 6000\,\text{kg}\cdot\text{m}^2$, unsprung wheel set mass $m_w = 1800\,\text{kg}$, total axle load $P = 140.1\,\text{kN}$, distance between the axles $l_w = 2.7\,\text{m}$, distance between the centre of bogies $l_b = 19\,\text{m}$, overall vehicle length $l = 26.6\,\text{m}$, primary suspension stiffness $k_1 = 2.4\,\text{MN/m}$, primary suspension viscous damping $c_1 = 30\,\text{kN}\cdot\text{s/m}$, secondary suspension stiffness $k_2 = 0.6\,\text{MN/m}$, secondary suspension viscous damping $c_2 = 20\,\text{kN}\cdot\text{s/m}$ and the contact stiffness per wheel is $k_H = 1462.5\,\text{MN/m}$.

4.1 *Rail receptances*

The rail receptance has been calculated using the two prediction models introduced in Section 2.2. For the soil of the Horstwalde the rail receptance was calculated for a stationary load, a moving load at speed $v = 150$ km/h (41.66 m/s) and a moving load at speed $v = 300$ km/h. For the stationary load the rail receptance is calculated using Eq. (14) for a single unit load $(P_l(\omega) = 1)$ at $x = \alpha_l$. The receptances for moving load cases are calculated in the same way but using Eq. (19). The amplitude and phase of rail receptances are shown in Figure 4. As the ground at Horstwalde is homogeneous, the rail receptance has an almost constant magnitude with frequency, decreasing slightly above 50 Hz.

Figure 5 gives the amplitude and phase of rail receptances for the Greby site where it is calculated for a stationary load and a moving load at 150 km/h. For the stationary load there is peak at about 11 Hz caused by the ground layering. This peak is appearing at a lower frequency about 9 Hz for the case of the moving load.

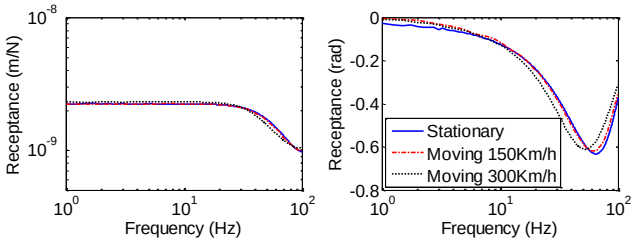

Figure 4. Magnitude (a) and phase (b) of rail receptance for Horstwalde site.

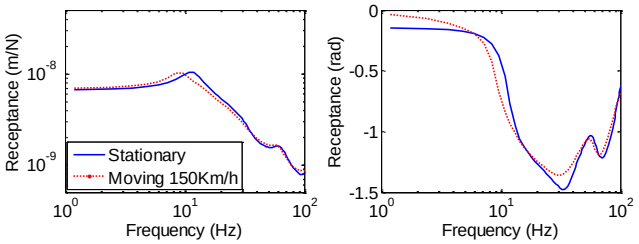

Figure 5. Magnitude (a) and phase (b) of rail receptance for Greby site.

4.2 *Dynamic rail and ground vibration*

The one third octave band spectra of the dynamic loads are shown in Figure 6 for the case of Horstwalde site. Comparing the spectra of the loads between the moving roughness model (MR) and the full model show excellent agreement. The MR model that has not included the axle correlation (see Eq. (28)) shows differences, as shown in Figure 6. For validation reasons results from a moving roughness coupled 2.5D finite element/boundary element model developed in [6] are presented. The motion of the train is included only in the full model but this difference does not appear significant. The results in Figure 6a correspond to the leading wheelset of a bogie. Results for the trailing wheelset are shown in Figure 6b and can be seen to be higher over the frequency range 1.6-6.3 Hz.

Figure 7 gives the one third octave band spectra of the dynamic loads for the case of the Greby site, where the MR model is compared with the uncorrelated MR model and the full model. The agreement is very similar with that in Figure 6. Additionally there should be noted that comparing the spectra simulated for the Horstwalde site in Figure 6 with the spectra of Greby site in Figure 7 there are no significant differences meaning that the properties of the soil are not very important when calculating the forces on the rails, at least for the specific range of frequencies 0 to 100 Hz.

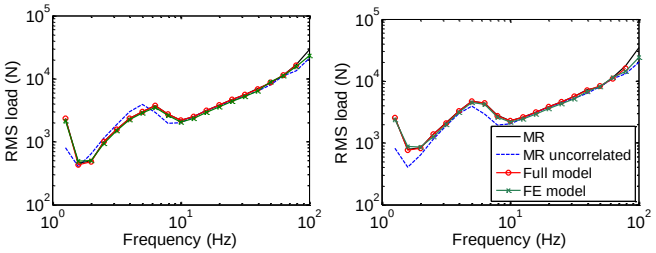

Figure 6. 1/OB load spectrum for Horstwalde for moving roughness approach (MR), uncorrelated axles case, full model and FE model; (a) leading wheelset, (b) second wheelset.

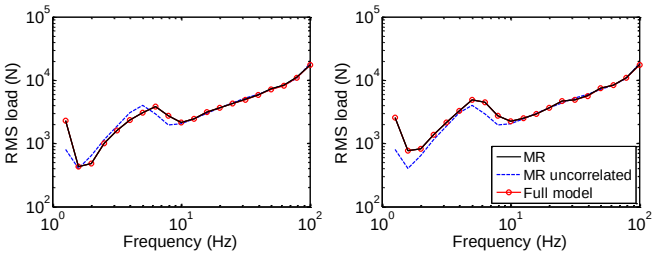

Figure 7. 1/3 OB load spectrum for Greby for moving roughness approach (MR), uncorrelated axles case and full model; (a) leading wheelset, (b) second wheelset.

For the dynamic response of the rail one third octave band results are shown in Figure 8 for both soil types. For the Horstwalde site in Figure 8a, the vibration level is predicted by four different models, the MR model, the uncorrelated MR model, the full model that works in the moving frame and the available FE/BE model. In each case the results are the average vibration during the passage of the train, including the full pass-by but normalised to the pass-by duration corresponding to the train length. The motion of the train is included only in the full model. The three MR models show the same trends with the full model, although lacking some of the spectral detail. Analogous results are shown in Figure 8b for the rail vibration level predicted by the model simulating the Greby site and presented for the MR model, the MR uncorrelated model and the full model. Comparing the two different soil models it can be seen that the vibration level is higher at the Greby site about 5 to 16 dB for low frequencies up to 40 Hz. At frequencies higher than 40 Hz the response calculated for Horstwalde site is about 4-7 dB higher.

In terms of computational effort, it seems that the MR approach is less demanding in computational effort. This advantage arises from fact that the full model takes into account the coupling between the moving load and the receiving point in the free field or at the rail. Thus, a dense

sequence of receiving frequencies has to be calculated in order to fully describe the narrow band of receiving frequencies for each excitation frequency. MR approach instead calculates one receiving frequency for each excitation frequency of the irregularity. Figure 9 shows the narrow band velocity spectrum at the rail for the Horstwalde site where the complexity of the full model response is compared with the response predicted by the MR approach. Moreover, for the MR approach the response in the wavenumber domain is symmetric in *x* and *y* direction with respect to the load.

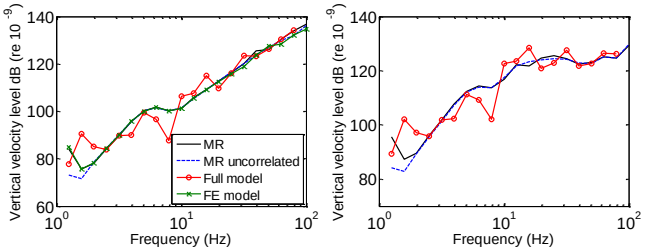

Figure 8. 1/3 OB dynamic velocity response level; (a) Horstwalde, (b) Greby.

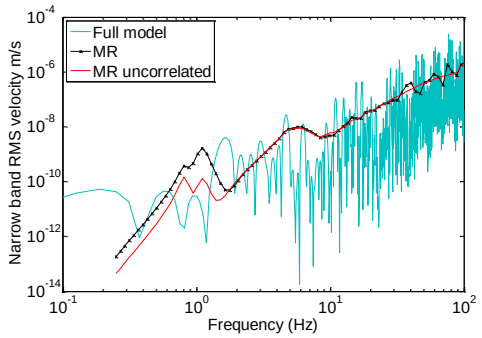

Figure 9. Narrow band dynamic velocity response at the rail for Horstwalde site.

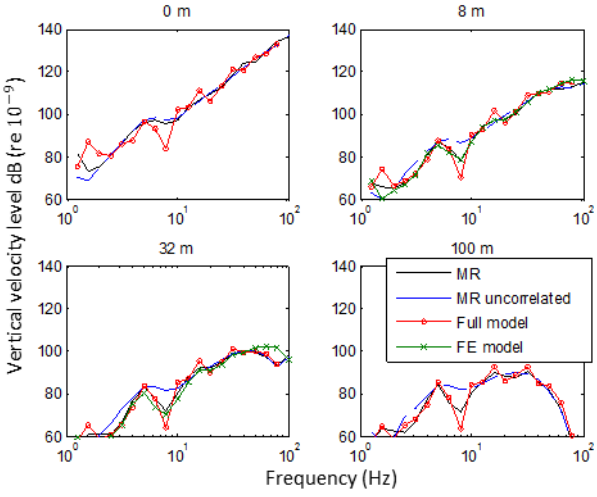

Figure 10. 1/3 OB dynamic velocity response level in the Horstwalde free field; (a) 0 m, (b) 8 m, (c) 32 m and (d) 100 m from the track.

Figure 10 shows the dynamic response in the free field for the Horstwalde site at distances of 0 m (under the track), 8 m, 32 m and 100 m from the track. The response normalized by the pass-by time velocity is predicted by four different models, the MR model, the uncorrelated MR model, the full model and the FE/BE model (where the prediction is available only for the distances of 8 m and 32 m from the track). The results are displayed in one third octave bands. Similarly with the rail vibration the three MR models show the same trends with the full model, but they lack some of the spectral detail.

CONCLUSIONS

Two different approaches were used to calculate the vibration PSD of the rail and in the free field from a train moving on a surface railway track at a constant velocity. For both methodologies it is assumed that each wheel is excited by the same roughness apart from a time lag. The two approaches use the PSD of the track unevenness along with TFs of the track and its supporting ground that are calculated using a well-developed 2.5D semi-analytical model which accounts for a ballasted track on the surface of a homogeneous layered half-space. The first approach is based on modelling the train at fixed position on the track and is excited by moving the roughness between the wheels and track with the velocity of train. In the second approach, the full model that includes the motion of the train is considered. For this model the response at a given frequency is a combination of responses induced by different excitation frequencies due to the Doppler effect in the ground. The two methods give the same predictions for the dynamic loads at the wheel-rail contact points with the moving roughness approach to be less demanding in computational effort. Comparing the vibration level predicted at the rail and in the free field, the full model approach, although more demanding in computational effort, show better spectral detail.

ACKNOWLEDGMENTS

This work has been supported by the EPSRC under the research grant EP/K006002/1, “MOTIV: Modelling of Train Induced Vibration”.

REFERENCES

[1] G. Lombaert, G. Degrande, S. Francois and D.J. Thompson, Ground-borne vibration due to railway traffic. *Proceedings of the 11th International Workshop on Railway Noise, IWRN11*, J. Nielsen et al. (Eds), Uddevalla, Sweden, 266-301, September 2013.

[2] X. Sheng, C.J.C. Jones, and D.J. Thompson. A theoretical model for ground vibration from trains generated by vertical track irregularities. *Journal of Sound and Vibration*, 272(3-5), 937–965, 2004.

[3] G. Lombaert and G. Degrande. Ground-borne vibration due to static and dynamic axle loads of InterCity and high speed trains. *Journal of Sound and Vibration*, 319(3-5), 1036–1066, 2009.

[4] X. Sheng, C.J.C. Jones and M. Petyt, Ground vibration generated by a harmonic load acting on a railway track. *Journal of Sound and Vibration*, 225(1), 3-28, 1999.

[5] X. Sheng, C.J.C. Jones, M. Petyt, Ground vibration generated by a load moving along a railway track. *Journal of Sound and Vibration*, 228 (1), 129–156, 1999.

[6] X. Sheng, C.J.C. Jones and D.J. Thompson, Prediction of ground vibration from trains using the wavenumber finite and boundary element methods, *Journal of Sound and Vibration*, 293, 575 – 586, 2006.

[7] J.A. Forrest and H.E.M. Hunt, Ground vibration generated by trains in underground tunnels. *Journal of Sound and Vibration*, 294,706–736, 2006.

[8] A.A. Mirza, A. Frid, J.C.O. Nielsen and C.J.C. Jones, Ground vibrations induced by railway traffic - the influence of vehicle parameters. *Proceedings of the 10th International Workshop on Railway Noise, IWRN10*, Nagahama, Japan, October 2010.

[9] V. Garg and R. Dukkipati. Dynamics of railway vehicle systems. Academic Press, Canada, 1984.